DC Voltage Oscillation Stability Analysis of DC-Voltage-Droop-Controlled Multiterminal DC Distribution System using Reduced-Order Modal Calculation

Qiang Fu, *Member, IEEE*, Wenjuan Du, *Member, IEEE*, Haifeng Wang, *Senior Member, IEEE*, Xiaoyang Ma, and Xianyong Xiao, *Senior Member, IEEE*

***Abstract*—To reduce the dimensions of a multiterminal DC (MTDC) distribution system connected with multiple voltage source converters (VSCs), a dynamic equivalent model is normally established, assuming that the VSCs are either identical or have a specified topology. These assumptions are inconsistent with practical scenarios, and thus, may lead to errors in the analyzed results. In this study, differences of the VSCs are considered, and a dynamic equivalent model of a DC-voltage-droop-controlled MTDC distribution system is established by reconstructing the dynamics of the VSCs and the DC network. Based on that, a dynamic-reconstruction-based reduced-order modal calculation method is proposed to quickly calculate the DC voltage oscillation mode and determine the stability. For a MTDC distribution system with N different VSCs, the highest dimension is $NH + T$, where the orders of the VSC and DC network are H and T, respectively. The highest dimension using the proposed method can be reduced to $H + 1$. Finally, the advances of the proposed method are demonstrated by comparing with other reduced-order methods. The conclusions are verified by both a simple example and a large-scale DC distribution system with 100 different VSCs.**

***Index Terms*—Dynamic reconstruction, DC voltage oscillation, MTDC distribution system, reduced-order modal calculation, stability analysis**

NOMENCLATURE

C_k : Capacitance on the DC side of the k^{th} VSC
$\overline{V}_k$: DC voltage of the k^{th} VSC
$\overline{I}_{netk}$: DC current at input C_k from the DC network
$\overline{I}_k$: DC current at output of C_k
P_k : Active power of the k^{th} VSC
C_{lj} : Capacitance on the DC side of the j^{th} DC load
$\overline{V}_{lj}$: DC voltage of the j^{th} DC load
$\overline{I}_{netlj}$: DC current at input C_{lj} from the DC network
$\overline{I}_{lj}$: DC current at output of C_{lj}
P_{lj} : Active power of the j^{th} DC load
X_k : Reactance of the filter on the AC side of the k^{th} VSC
$\tilde{I}_{dk}$: AC current in the d axis
$\tilde{I}_{qk}$: AC current in the q axis
$\tilde{V}_k$: AC voltage at the point of common coupling
$\tilde{V}_{dk}$: d–axis component of $\tilde{V}_k$
$\tilde{V}_{qk}$: q–axis component of $\tilde{V}_k$
$\tilde{V}_{ck}$: AC voltage at the terminal of the AC–DC converter
$\tilde{V}_{cdk}$: d–axis component of $\tilde{V}_{ck}$
$\tilde{V}_{cqk}$: q–axis component of $\tilde{V}_{ck}$
ω_0 : Synchronous frequency, 377 rad/s
$K_{pk} + K_{ik}s^{-1}$: Transfer function of the outer control loop of the k^{th} VSC
$K^c_{pk} + K^c_{ik}s^{-1}$: Transfer function of the inner control loop of the k^{th} VSC
Superscript *ref*: Reference value of the control system
Subscript k: Number identifier of all VSCs
Subscript j: Number identifier of the active power–controlled VSCs
ω_d : Frequency of DC voltage oscillation
$\mathbf{Y}_d(s)$: Original admittance matrix of the DC network
$R_{ek}(s)$: Original transfer function of the k^{th} VSC
$\mathbf{Y}_e(s)$: Dynamic constructed admittance matrix of the DC network
$R_0(s)$: Dynamic constructed transfer function of the VSCs
Δ : Small increment in variable
$\mathbf{E}$: Identity matrix
$\mathbf{0}$: Zero matrix

I. INTRODUCTION

Variable-speed drives, lighting, and electronics are key examples of systems in which load increases significantly with the development of distribution systems [1]–[2]. However, an extra energy conversion stage from AC to DC power is required before connecting to these DC loads, which reduces overall system efficiency. Using a DC distribution system to replace the AC distribution system can improve the efficiency by 10% – 22% in data centers, commercial, and residential sectors [3]–[4]. In addition, the issue of reactive power can be eliminated in the DC distribution system. Therefore, the DC distribution system is becoming increasingly attractive [5]–[6]. A multiterminal DC (MTDC) distribution system forms when a large number of loads and sources, such as solar photovoltaics and wind turbines, are connected through AC/DC converters [7]–[8]. So far, many practical MTDC distribution systems have been tested all over the world [9-10]. The MTDC distribution system in Zhuhai, China is proved to have good economic and commercial promotion values [11].

The dynamics of the MTDC distribution system are complex, which results in problems related to DC voltage regulation and power sharing [12]. The basic DC voltage control strategies can

This work is completed by the Engineering Special Team of Sichuan University on New Energy Power Systems and financially supported by the Natural Science Foundation of China under Grant 52077144.

Qiang Fu, Wenjuan Du, Haifeng Wang, Xiaoyang Ma, and Xianyong Xiao, are with electric engineering school of the Si chuan university, corresponding author is Wenjuan Du, Email: ddwenjuan@qq.com.

be classified into centralized, decentralized and distributed control [13]–[14]. Master-slave control is a representation of the centralized control that tightly relies on communications. The master VSC controls DC voltage and slave VSCs control active power. The observability and controllability are strong, but the reliability is low. Any breakdown of the master VSC or communication network can result in failure of the DC system [15]. Due to development of communication technologies, the distributed control is proposed. It can realize functions of the centralized control in a distributed way and thus improving the reliability [16]–[17]. However, it still relies on communication network, the used communication technologies, such as Zigbee, WiFi [17], are more appliable for a small-scale system. The DC voltage droop control is a typical example of the decentralized control that can realize the power sharing among VSCs and maintain the DC voltage [18]–[19]. It involves measurement of only the local variables and does not require communication for its operation. Therefore, it has high reliability, low cost, and easy scalability. Motivated by that, the VSCs in this study are equipped with the DC voltage droop control to autonomously regulate DC voltage of the MTDC distribution system [20].

The DC voltage oscillation is an example of power supply and balance stability, which is not one poorly tuned VSC, but the coordination of multiple VSCs [21]. DC voltage instability has been listed as one of stability issues of the DC distribution system [21]. The authors in [22] argued that unbalanced power is a major reason for DC voltage instability. Using the modal analysis method, occurrence of the DC voltage oscillation has been demonstrated [20], [23]–[25]. In which, the DC voltage oscillation mode is firstly calculated based on a state-space model. The DC voltage oscillation occurs if the DC voltage oscillation mode locates on right side of the complex plane. Then, the major parameters that affect DC voltage oscillation stability can be determined based on results of participation factors and sensitivity analysis. Therefore, calculating the DC voltage oscillation mode is a key step of DC voltage oscillation stability analysis.

To accurately analyze the DC voltage oscillation stability, comprehensive dynamics are generally considered, and a full-order state-space model is established [8]. However, full-order model is time-consuming for stability analysis, especially in a large-scale distribution system. Consequently, some methods of reduced-order model for modal analysis have been proposed. In [3], dynamics of converter control loops were ignored, and thus converters were considered to have ideal droop coefficients. In [26], dynamic performance of converters was assumed to be perfect, converters were considered as constant power sources or loads. Evidently, the simplifications can reduce dimensions of the MTDC distribution system. But instabilities caused by control loops of the converters cannot be detected. Hence, these reduced-order methods cannot be applied to analyze the DC voltage oscillation stability.

As the DC voltage oscillation stability was studied in-depth, it was found that fast dynamics generally had weak effects on DC voltage oscillation, so they can be ignored for simplification. In [23] and [27], authors indicated that response speeds of the inner current and DC voltage control loops are in different frequency ranges. The dynamics of the current control loop can be ignored when analyzing the DC voltage control. In [28]–[29], based on the singular perturbation theory, the state variables were divided into slow and fast dynamic variables, respectively. Compared with slow dynamic variables, fast dynamic variables were multiplied by extremely small coefficients, thus reducing its effects. This provided a numerical verification for ignoring the fast dynamics. However, total dimensions of the MTDC distribution system increases with the increase in the number of converters. Curse of dimensionality still occurs if the number of converters is large.

To solve the issue of high-dimensionality caused by increase in number of converters, another type of reduced-order method aggregated multiple converters into an equivalent converter. Using this method, the dimensions of the MTDC distribution system can not only be significantly reduced, but also increases slowly as the number of converters increases. To date, two main categories of these methods have been proposed: the capacity-weighted mean value (CMV) and parameter identification (PI) methods. A reduced-order model obtained using the CMV method mainly considers the equivalence of the converters' generating capability, without fully considering the impact of topology [30]–[32]. The PI method may be used to fully consider the impact of topology, but it is sensitive to variations in operating conditions [33]–[35]. To fill the gaps of CMV and PI, a new reduced-order modal computation method was proposed in [36]. This was demonstrated to be more accurate and faster than the CMV and PI methods. However, these methods have not been applied to analyze the DC voltage oscillation stability of the MTDC distribution system.

The defect of previously proposed reduced-order methods [30]–[36] is that they cannot calculate modes by simultaneously considering differences in the equipment and variations in the network topology. The assumptions that VSCs are either identical or have a specified topology differ from a real-world scenario and may result in errors in the analyzed results. This study follows the method of [36] and proposes an advanced reduced-order modal calculation method that can overcome the previously mentioned defect. First, a dynamic reconstruction technique of the MTDC distribution system that considers the differences of multiple VSCs is proposed. Second, a dynamic reconstruction-based reduced-order modal calculation method is proposed. It can calculate the DC voltage oscillation mode rapidly and accurately even if network topologies, operating states, and control parameters of VSCs are different. Third, the advances of the proposed method were verified by comparing with the methods based on the full-order model, ideal dynamic model [3], and singular perturbation theory-based model [29].

The rest of this manuscript is organized as follows: Section II describes a linearized model of the MTDC distribution system. In Section III, the dynamic reconstruction-based reduced-order modal calculation method is proposed. The theoretical accuracy is verified and the advantages over other reduced-order methods are demonstrated. In Section IV and V, the advantages of the proposed method are numerically verified using both a small- and a large-scale MTDC distribution system. In Section VI, the conclusions and contributions of the study are summarized.

II. Linearized Model of a MTDC Distribution System

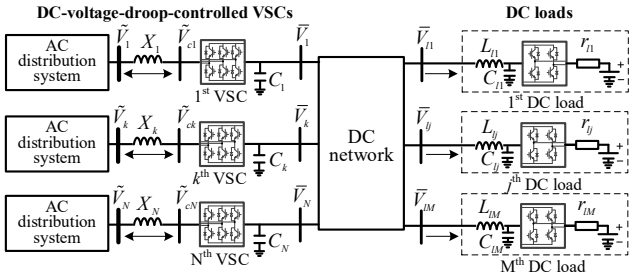

Fig. 1. Configuration of a DC-voltage-droop-controlled MTDC distribution system.

The configuration of a MTDC distribution system with N VSCs and M DC loads is shown in Fig. 1 [8]. The k^{th} VSC adopts DC voltage droop control to maintain DC voltage stability, where k = 1, 2,…, N. The DC-DC converter of the j^{th} DC load adopts active power control to maintain the constant power of the DC load, j = 1, 2,…, M. Unlike [8], N VSCs are connected to grid-connected AC distribution systems, so the VSCs do not participate in control of the AC frequency. The power flow between AC and DC distribution systems are bi-directional, i.e., AC distribution systems can delivery power to DC loads or exchange power through the DC network. The power flow between the DC network and loads is unidirectional. Directions of the power flow are indicated by arrows.

A. Transfer Function of DC-Voltage-Droop-Controlled VSC

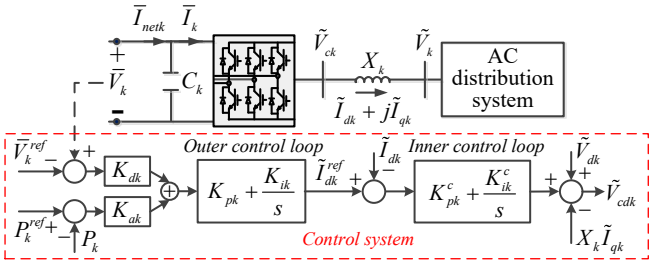

Fig. 2. Configuration of the DC voltage droop control of the k^{th} VSC.

Fig. 2 shows a general representation of the DC voltage droop control of the k^{th} VSC [12]. It is same as that in [20] when $K_{dk}=1$ and is same as that in [8] when $K_{ak}=1$. Thus, the function of power sharing can be realized by adjusting K_{ak} and K_{dk}. The positive direction of the variable is defined as the input direction of VSCs and indicated by arrows. If power flow follows positive direction, variables such as currents and power are positive. Otherwise, the variables are negative.

Assuming that the direction of $\tilde{V}_k$ is along the d axis of the VSC d–q coordinate system (i.e., $\tilde{V}_{qk}=0$, $\tilde{V}_{dk}=\tilde{V}_k$), yields

$$P_k=\tilde{V}_k\tilde{I}_{dk}=\bar{V}_k\bar{I}_k. \tag{1}$$

The dynamic equation of the DC voltage is given as follows:

$$C_k\frac{d\bar{V}_k}{dt}=\bar{I}_{netk}-\bar{I}_k. \tag{2}$$

The dynamic equation of the AC current in the d axis is:

$$X_k\omega_0^{-1}\frac{d\tilde{I}_{dk}}{dt}=X_k\tilde{I}_{qk}+\tilde{V}_k-\tilde{V}_{cdk}. \tag{3}$$

The dynamic equation of the inner control loop is obtained from Fig. 2, and expressed as follows:

$$\tilde{V}_{cdk}=\tilde{V}_k-X_k\tilde{I}_{qk}+\left(K_{pk}^c+K_{ik}^cs^{-1}\right)\left(\tilde{I}_{dk}^{ref}-\tilde{I}_{dk}\right). \tag{4}$$

Substituting (4) into (3) yields:

$$\tilde{I}_{dk}=G_{ik}(s)\tilde{I}_{dk}^{ref}. \tag{5}$$

where $G_{ik}(s)=\dfrac{K_{pk}^cs+K_{ik}^c}{X_k\omega_0^{-1}s^2+K_{pk}^cs+K_{ik}^c}$.

In (5), $G_{ik}(s)$ represents the dynamics of the inner current loop. As shown in Fig. 2, the transfer function of the outer control loop of the VSC can be obtained:

$$\tilde{I}_{dk}^{ref}=\left(K_{pk}+\frac{K_{ik}}{s}\right)\left(K_{dk}\left(\bar{V}_k-\bar{V}_k^{ref}\right)+K_{ak}\left(P_k^{ref}-P_k\right)\right). \tag{6}$$

By linearizing (1), (2), (5), and (6) at a steady state, the transfer function model of the k^{th} VSC is obtained:

$$\Delta\bar{V}_k=R_{ek}(s)\Delta\bar{I}_{netk}+G_{vk}(s)\Delta\tilde{V}_k. \tag{7}$$

where $R_{ek}(s)=\dfrac{z_{1,k}(s)s+z_{2,k}(s)}{g_{1,k}(s)s^2+g_{2,k}(s)s+g_{3,k}(s)}$,

$$G_{vk}(s)=-\frac{\tilde{I}_{dk,0}}{g_{1,k}(s)s^2+g_{2,k}(s)s+g_{3,k}(s)},$$

$$z_{1,k}(s)=\bar{V}_{k,0}+\bar{V}_{k,0}\tilde{V}_{k,0}K_{ak}K_{pk}G_{ik}(s),$$

$$z_{2,k}(s)=\bar{V}_{k,0}\tilde{V}_{k,0}K_{ak}K_{ik}G_{ik}(s),$$

$$g_{1,k}(s)=C_k\bar{V}_{k,0}+C_k\bar{V}_{k,0}\tilde{V}_{k,0}K_{pk}K_{ak}G_{ik}(s),$$

$$g_{2,k}(s)=C_k\bar{V}_{k,0}\tilde{V}_{k,0}K_{ik}K_{ak}G_{ik}(s)+G_{ik}(s)K_{pk}\tilde{V}_{k,0}K_{dk}-\bar{I}_{k,0}\tilde{V}_{k,0}K_{pk}K_{ak}G_{ik}(s)-\bar{I}_{k,0},$$

$$g_{3,k}(s)=\tilde{V}_{k,0}K_{ik}K_{dk}G_{ik}(s)-\bar{I}_{k,0}\tilde{V}_{k,0}K_{ik}K_{ak}G_{ik}(s).$$

Equation (7) shows that dynamics of the AC distribution system affect the MTDC distribution system through $\Delta\tilde{V}_k$. The effects of the energy sources or storage in the AC distribution system can be analyzed if their transfer function $E_k(s)=\Delta\tilde{V}_k/\Delta\bar{I}_{netk}$ is derived. As affected by $E_k(s)$, the dynamic transfer function of a VSC is changed from $R_{ek}(s)$ to be $R_{ek}(s)+G_{vk}(s)E_k(s)$. Thus, the effects of the equipment in the AC distribution system on the MTDC distribution system can be determined by analyzing $G_{vk}(s)E_k(s)$, which is similar to $\Delta R_{e2,k}(s)$ in section III B. Considering that the present study focuses on small-signal DC voltage oscillation stability within the grid-connected MTDC distribution system, the capacity of the AC distribution systems is so much larger than that of the MTDC distribution system that they can be represented by infinite buses. The dynamics of the AC distribution systems are therefore ignored, and the AC voltages at the point of common coupling (PCC) nodes are kept constant, $\Delta\tilde{V}_k=0$. Therefore, in analyzing the DC voltage oscillation stability within the MTDC distribution system, (7) can be rewritten as follows:

$$\Delta \bar{V}_k = R_{ek}(s)\Delta \bar{I}_{netk}. \quad (8)$$

B. Transfer Function of DC Loads

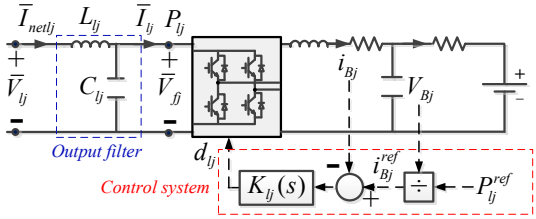

Fig. 3. Configuration of the active power control of the j^{th} DC-DC converter.

In Fig. 3, the DC-DC converter is used to deliver power to the DC load that is represented by a DC voltage source and a series-connected resistance [26]. Filter is installed to eliminate harmonics and the active power control is adopted to control the transmitted power as a constant.

For the circuit in Fig. 3, the following voltage and current equations can be obtained:

$$\bar{V}_{lj} = L_{lj}\frac{d\bar{I}_{netlj}}{dt} + \bar{V}_{fj}, \bar{I}_{netlj} = \frac{P_{lj}}{\bar{V}_{fj}} + C_{lj}\frac{d\bar{V}_{fj}}{dt} \quad (9)$$

Considering the fast and accurate current-control loop of the active power control of the j^{th} DC-DC converter, the output power of the DC-DC converter is almost equal to the power reference value, i.e., with constant power loads and $\Delta P_{lj} = 0$ [26]. From Fig. 3 and (8), the transfer function of the j^{th} DC load is obtained as follows:

$$\Delta \bar{V}_{lj} = L_{lj}s + \frac{\bar{V}_{lj,0}^{\ 2}}{C_{lj}s\bar{V}_{lj,0}^{\ 2} - P_{lj,0}}\Delta \bar{I}_{netlj} = R_{lj}(s)\Delta \bar{I}_{netlj}. \quad (10)$$

C. Transfer Function Model of the MTDC Distribution System

In MTDC distribution systems, common architectures of the DC network are single bus and multi-bus configurations, which are simple and have been widely analyzed in studies [10, 37]. To enhance security of the critical load, ring bus and hybrid configurations are adopted [20, 38], increasing the complexity of the MTDC distribution system. Also, the parameters, such as R/X ratios, impedance ranges, of the networks can be different. To address this issue, a generalized transfer function of the DC network without any assumption on topologies and parameters is used. Denoting the dynamic admittance matrix of the DC network indicated in Fig. 1 as $\mathbf{Y}_{net}(s)$, yields:

$$\begin{bmatrix}\bar{\mathbf{I}}_d\\ \bar{\mathbf{I}}_l\\ \mathbf{0}\end{bmatrix} = -\mathbf{Y}_{net}(s)\begin{bmatrix}\bar{\mathbf{V}}_d\\ \bar{\mathbf{V}}_l\\ \bar{\mathbf{V}}_r\end{bmatrix} = -\begin{bmatrix}\mathbf{Y}_{11}(s) & \mathbf{Y}_{12}(s) & \mathbf{Y}_{13}(s)\\ \mathbf{Y}_{21}(s) & \mathbf{Y}_{22}(s) & \mathbf{Y}_{23}(s)\\ \mathbf{Y}_{31}(s) & \mathbf{Y}_{32}(s) & \mathbf{Y}_{33}(s)\end{bmatrix}\begin{bmatrix}\bar{\mathbf{V}}_d\\ \bar{\mathbf{V}}_l\\ \bar{\mathbf{V}}_r\end{bmatrix}. \quad (11)$$

where $\bar{\mathbf{I}}_d = [\Delta \bar{I}_{net1} \ldots \Delta \bar{I}_{netN}]^T$ and $\bar{\mathbf{V}}_d = [\Delta \bar{V}_{net1} \ldots \Delta \bar{V}_{netN}]^T$ are vectors that contain injected currents and the DC voltages of the VSCs, respectively. $\bar{\mathbf{I}}_l = [\Delta \bar{I}_{netl1} \ldots \Delta \bar{I}_{netlM}]^T$ and $\bar{\mathbf{V}}_l = [\Delta \bar{V}_{netl1} \ldots \Delta \bar{V}_{netlM}]^T$ are vectors that contain injected currents and the DC voltages of the DC loads, respectively. $\bar{\mathbf{V}}_r$ is a vector that contains the DC voltages at the remaining DC nodes.

According to (10), the transfer function of M DC loads is obtained:

$$\bar{\mathbf{I}}_l = \mathbf{Y}_l(s)\bar{\mathbf{V}}_l. \quad (12)$$

where $\mathbf{Y}_l(s) = \begin{bmatrix} R_{l1}(s)^{-1} & 0 & 0\\ 0 & \ddots & 0\\ 0 & 0 & R_{lM}(s)^{-1}\end{bmatrix}$.

Substituting (12) in to (11), yields:

$$\begin{bmatrix}\bar{\mathbf{I}}_d\\ \mathbf{0}\\ \mathbf{0}\end{bmatrix} = -\begin{bmatrix}\mathbf{Y}_{11}(s) & \mathbf{Y}_{12}(s) & \mathbf{Y}_{13}(s)\\ \mathbf{Y}_{21}(s) & \mathbf{Y}_{22}(s)+\mathbf{Y}_l(s) & \mathbf{Y}_{23}(s)\\ \mathbf{Y}_{31}(s) & \mathbf{Y}_{32}(s) & \mathbf{Y}_{33}(s)\end{bmatrix}\begin{bmatrix}\bar{\mathbf{V}}_d\\ \bar{\mathbf{V}}_l\\ \bar{\mathbf{V}}_r\end{bmatrix}. \quad (13)$$

From (13), the transfer function between $\bar{\mathbf{I}}_d$ and $\bar{\mathbf{V}}_d$ can be obtained by eliminating $\bar{\mathbf{V}}_l$ and $\bar{\mathbf{V}}_r$:

$$\bar{\mathbf{I}}_d = -\mathbf{Y}_d(s)\bar{\mathbf{V}}_d. \quad (14)$$

where $\mathbf{Y}_d(s) = \mathbf{Y}_{11}(s) - \begin{bmatrix}\mathbf{Y}_{12}(s) & \mathbf{Y}_{13}(s)\end{bmatrix}\begin{bmatrix}\mathbf{Y}_{22}(s)+\mathbf{Y}_l(s) & \mathbf{Y}_{23}(s)\\ \mathbf{Y}_{32}(s) & \mathbf{Y}_{33}(s)\end{bmatrix}^{-1}\begin{bmatrix}\mathbf{Y}_{21}(s)\\ \mathbf{Y}_{31}(s)\end{bmatrix}$.

Substituting (8) into (14), the transfer function model of the MTDC distribution system is obtained:

$$\mathbf{Y}_d(s)\mathbf{F}_d(s) + \mathbf{E} = \mathbf{0} \quad (15)$$

where $\mathbf{F}_d(s) = \begin{bmatrix} R_{e1}(s) & 0 & 0\\ 0 & \ddots & 0\\ 0 & 0 & R_{eN}(s)\end{bmatrix}$.

Based on the multiple high-order dynamic equations of (15), the DC voltage oscillation mode can be calculated to evaluate the DC voltage oscillation stability of the MTDC distribution system. The highest order of the transfer function model is $NH+T$, where the orders of the DC-voltage-droop-controlled VSC and the DC network are H and T, respectively.

III. Dynamic Reconstruction of the MTDC Distribution System

A. Brief introduction of the old method proposed in [36]

In [36], the differences among N VSCs are ignored and thus assuming all VSCs are same as the standard VSC. The transfer function of the standard VSC is as follows:

$$\Delta \bar{V}_k = \frac{z_{1,0}(s)s + z_{2,0}(s)}{g_{1,0}(s)s^2 + g_{2,0}(s)s + g_{3,0}(s)} = R_{e0}(s)\Delta \bar{I}_{netk} \quad (16)$$

With this assumption, the transfer function model in (15) can be simplified as

$$\mathbf{Y}_d(s)\mathbf{F}_e(s) + \mathbf{E} = \mathbf{0}. \quad (17)$$

where $\mathbf{F}_e(s) = \begin{bmatrix} R_{e0}(s) & 0 & 0\\ 0 & \ddots & 0\\ 0 & 0 & R_{e0}(s)\end{bmatrix}$.

Equation (17) can be proven to be equal to multiple sub-

equations at DC voltage oscillation frequency (see Appendix A for more details). The DC voltage oscillation stability can be determined by

$$R_{e0}(s)\left[\rho_{R0}+\rho_{M0}s\right]+1=0 \tag{18}$$

where ρ_0 is an eigenvalue of $\mathbf{Y}_d(\omega_d)$ corresponding to the DC voltage oscillation mode. $\rho_{R0}=\mathrm{Re}[\rho_0]$, $\rho_{M0}=\mathrm{Im}[\rho_0]/\omega_d$.

The highest calculational order of the system is reduced from *NH+T* to *H+1* based on (18). However, the assumption made in (16) and (17) may cause significant errors when the differences among *N* VSCs cannot be neglected. Therefore, to solve this issue, dynamic-reconstruction-based modal calculation method is proposed in subsections B – D.

B. Dynamic Reconstruction of N VSCs

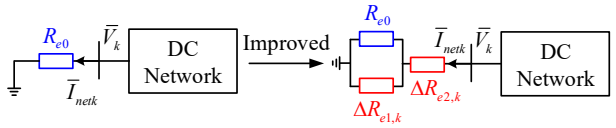

(a) Differences are ignored (b) Differences are considered

Fig. 4. Dynamic reconstruction of the k^{th} VSC.

The coefficients corresponding to the differences of the k^{th} VSC can be defined by the following equations:

$$\begin{aligned}\Delta z_{1,k}(s)&=z_{1,k}(s)-z_{1,0}(s)\\ \Delta z_{2,k}(s)&=z_{2,k}(s)-z_{2,0}(s)\end{aligned}\quad\begin{aligned}\Delta g_{1,k}(s)&=g_{1,k}(s)-g_{1,0}(s)\\ \Delta g_{2,k}(s)&=g_{2,k}(s)-g_{2,0}(s)\\ \Delta g_{3,k}(s)&=g_{3,k}(s)-g_{3,0}(s)\end{aligned}. \tag{19}$$

Accordingly, the dynamics of the k^{th} VSC are reconstructed as follows:

$$R_{ek}(s)=\frac{1}{\dfrac{1}{R_{e0}(s)}+\dfrac{1}{\Delta R_{e1,k}(s)}}+\Delta R_{e2,k}(s), \tag{20}$$

where

$$R_{e0}(s)=\frac{z_{1,0}(s)s+z_{2,0}(s)}{g_{1,0}(s)s^2+g_{2,0}(s)s+g_{3,0}(s)}$$

$$\Delta R_{e1,k}(s)=\frac{z_{1,0}(s)s+z_{2,0}(s)}{\Delta g_{1,k}(s)s^2+\Delta g_{2,k}(s)s+\Delta g_{3,k}(s)}.$$

$$\Delta R_{e2,k}(s)=\frac{\Delta z_{1,k}(s)s+\Delta z_{2,k}(s)}{g_{1,k}(s)s^2+g_{2,k}(s)s+g_{3,k}(s)}$$

Equation (20) indicates that the reconstructed dynamics of the k^{th} VSC consist of three parts, $R_{e0}(s)$, $\Delta R_{e1,k}(s)$, and $\Delta R_{e2,k}(s)$. $R_{e0}(s)$ represents the dynamics of the standard VSC, $\Delta R_{e1,k}(s)$ and $\Delta R_{e2,k}(s)$ represent the dynamics caused by the differences of the k^{th} VSC. The configuration of the reconstructed VSC is illustrated in Fig. 4. Equation (20) and Fig. 4 show that $\Delta R_{e1,k}(s)$ is caused by $\Delta g_{1,k}(s)$, $\Delta g_{2,k}(s)$, and $\Delta g_{3,k}(s)$, and is equal to a dynamic impedance connected to $R_{e0}(s)$ in parallel. $\Delta R_{e2,k}(s)$ is caused by $\Delta z_{1,k}(s)$ and $\Delta z_{2,k}(s)$, and is equal to a dynamic impedance connected to $R_{e0}(s)$ in series. Therefore, the physical meaning and the effects of the differences caused by different coefficients are clarified. Comparing Fig. 4 (a) with Fig. 4 (b) shows that ignoring the differences may change the equivalent dynamic impedance of a VSC, which is the reason for the errors caused by the old method.

C. Dynamic Reconstruction of DC Network

$\Delta R_{e1,k}(s)$ and $\Delta R_{e2,k}(s)$ change the impedance of the DC transmission line connected from the k^{th} standard VSC to the DC network. Fig. 1 shows that the k^{th} VSC connects to the k^{th} DC node, denoting that the k^{th} DC node connects to the w^{th} DC node, $\Delta R_{e1,k}(s)$ changes the self–admittance of the k^{th} DC node and $\Delta R_{e2,k}(s)$ changes the self–admittances of the k^{th} and w^{th}

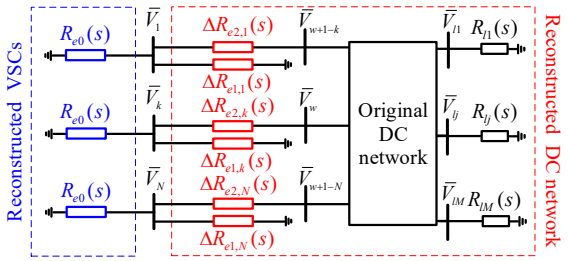

Fig. 5. Dynamic reconstruction of the DC network.

DC nodes and the mutual admittance between the k^{th} and w^{th} DC nodes. The reconstructed and original DC networks are indicated by red and black lines, respectively, in Fig. 5.

Considering $\Delta R_{e1,k}(s)$ and $\Delta R_{e2,k}(s)$ of all the VSCs, the reconstructed admittance matrix of the DC network is derived from (13) and Fig. 5 to be:

$$\begin{bmatrix}\bar{\mathbf{I}}_d\\ \mathbf{0}\\ \mathbf{0}\end{bmatrix}=-\begin{bmatrix}\mathbf{Y}_{11}(s)+\Delta\mathbf{Y}_{e1}(s)+\Delta\mathbf{Y}_{e2}(s), & \mathbf{Y}_{12}(s), & \mathbf{Y}_{13}(s)-\Delta\mathbf{Y}_{e3}(s)\\ \mathbf{Y}_{21}(s), & \mathbf{Y}_{22}(s)+\mathbf{Y}_l(s), & \mathbf{Y}_{23}(s)\\ \mathbf{Y}_{31}(s)-\Delta\mathbf{Y}_{e3}(s)^T, & \mathbf{Y}_{32}(s), & \mathbf{Y}_{33}(s)+\Delta\mathbf{Y}_{e4}(s)\end{bmatrix}\begin{bmatrix}\bar{\mathbf{V}}_d\\ \bar{\mathbf{V}}_l\\ \bar{\mathbf{V}}_r\end{bmatrix}. \tag{21}$$

where $\Delta\mathbf{Y}_{e1}(s)=\begin{bmatrix}\Delta R_{e1,k}(s)^{-1} & 0 & 0\\ 0 & \ddots & 0\\ 0 & 0 & \Delta R_{e1,N}(s)^{-1}\end{bmatrix}$,

$\Delta\mathbf{Y}_{e2}(s)$, $\Delta\mathbf{Y}_{e3}(s)$, and $\Delta\mathbf{Y}_{e4}(s)$ correspond to variations in the admittance matrix caused by the $\Delta R_{e2,k}(s)^{-1}$ of *N* VSCs. For example, considering that the k^{th} VSC connects to the w^{th} DC node, $-\Delta R_{e2,k}(s)^{-1}$ should be added to the k^{th} column, w^{th} row and k^{th} row, w^{th} column of the admittance matrix, and $\Delta R_{e2,k}(s)^{-1}$ should be added to the k^{th} column, k^{th} row and w^{th} row, w^{th} column of the admittance matrix.

From (21), the transfer function between $\bar{\mathbf{I}}_d$ and $\bar{\mathbf{V}}_d$ can be obtained by eliminating $\bar{\mathbf{V}}_l$ and $\bar{\mathbf{V}}_r$:

$$\bar{\mathbf{I}}_d=-\mathbf{Y}_e(s)\bar{\mathbf{V}}_d. \tag{22}$$

$$\mathbf{Y}_e(s)=\mathbf{Y}_{11}(s)+\Delta\mathbf{Y}_{e1}(s)+\Delta\mathbf{Y}_{e2}(s)-\begin{bmatrix}\mathbf{Y}_{12}(s) & \mathbf{Y}_{13}(s)-\Delta\mathbf{Y}_{e3}(s)\end{bmatrix}$$

where $\begin{bmatrix}\mathbf{Y}_{22}(s)+\mathbf{Y}_l(s) & \mathbf{Y}_{23}(s)\\ \mathbf{Y}_{32}(s) & \mathbf{Y}_{33}(s)+\Delta\mathbf{Y}_{e4}(s)\end{bmatrix}^{-1}\begin{bmatrix}\mathbf{Y}_{21}(s)\\ \mathbf{Y}_{31}(s)-\Delta\mathbf{Y}_{e3}(s)^T\end{bmatrix}$.

D. Reduced-order Calculation of DC Voltage Oscillation Mode

According to (20), (22), and Fig. 5, the transfer function model of the reconstructed MTDC distribution system is

obtained as follows:

$$\mathbf{Y}_e(s)\mathbf{F}_e(s)+\mathbf{E}=\mathbf{0}. \tag{23}$$

In contrast to (17), the DC voltage oscillation mode calculated using (23) is equal to that using (15), because the dynamics are included in the dynamic reconstruction technique instead of being ignored. Thus, the calculated results of (23) are more accurate than those of (17).

Based on the derivations in Appendix A and (23), the DC voltage oscillation stability can be determined by

$$R_{e0}(s)\left[\rho_{Rd}+\rho_{Md}s\right]+1=0 \tag{24}$$

where ρ_d is the k^{th} eigenvalue of $\mathbf{Y}_e(\omega_d)$ corresponding to the DC voltage oscillation mode. $\rho_{Rd}=\mathrm{Re}[\rho_d]$, $\rho_{Md}=\mathrm{Im}[\rho_d]/\omega_d$.

The characteristic equation of (24) is:

$$\begin{aligned}&\left[z_{1,0}(s)\rho_{Md}+g_{1,0}(s)\right]s^2+z_{2,0}(s)\rho_{Rd}+g_{3,0}(s)\\&+\left[z_{2,0}(s)\rho_{Md}+z_{1,0}(s)\rho_{Rd}+g_{2,0}(s)\right]s=0\end{aligned}. \tag{25}$$

Equation (25) show that, without the assumptions in (16), the highest calculational order of the system can also be reduced from *NH+T* to *H+1*.

E. Accuracy of the proposed method

Considering elements of $\mathbf{Y}_e(s)$ are complex, the first-order Taylor expansion equation is used to approximately represent $\mathbf{Y}_e(s)$ to analyze the accuracy of the method [39], yields

$$\mathbf{Y}_e(s)\approx\mathbf{Y}_{e0}+\mathbf{Y}_{e1}s. \tag{26}$$

where $\mathbf{Y}_{e0}=\mathbf{Y}_e(s)|_{s=0}$, $\mathbf{Y}_{e1}=\dfrac{\partial\mathbf{Y}_e(s)}{\partial s}|_{s=0}$.

The actual DC voltage oscillation mode is defined as $\lambda_d=-\varepsilon_d+j\omega_d$. Thus (23) can be strictly rewritten as

$$\begin{aligned}&\left(\mathbf{Y}_{e0}+\mathbf{Y}_{e1}s\right)\mathbf{F}_e(s)+\mathbf{E}\\&=\left(\mathbf{Y}_{e0}+\mathbf{Y}_{e1}\lambda_d\right)\mathbf{F}_e(s)+\mathbf{E}\\&=\left(\mathbf{Y}_{e0}-\mathbf{Y}_{e1}\varepsilon_d+j\mathbf{Y}_{e1}\omega_d\right)\mathbf{F}_e(s)+\mathbf{E}=\mathbf{0}\end{aligned} \tag{27}$$

In (27), ε_d determines whether the DC distribution system is stable or not, which varies significantly when operating state of the DC distribution system changes, so it is unknown before conducting the calculation. ω_d represents the frequency of the DC voltage oscillation, which is in a constant range and varies slightly as affected by operating states. Therefore, ω_d can be easily obtained by FFT analysis in similar scenarios. When the system has a risk of DC voltage oscillation, the damping of λ_d is weak such that $\varepsilon_d\ll\omega_d$. Under this condition, effects of $\mathbf{Y}_{e1}\varepsilon_d$ are much less than that of $\mathbf{Y}_{e1}\omega_d$, the error caused by ignoring $\mathbf{Y}_{e1}\varepsilon_d$ is small. In stability analysis, the weak-damping DC voltage oscillation mode is mainly focused, which is the reason for using $s=j\omega_d$ replaces $s=\lambda_d$ in deriving (24). When determining critical stability of the system, the damping of λ_d is zero such that $\varepsilon_d=0$. Under this condition, $s=\lambda_d=j\omega_d$, using this method to determine the stability cannot result in any error. Therefore, the proposed method is effective in calculating the weak-damping DC voltage oscillation mode and is accurate to determine the DC voltage oscillation stability. Multiply $\mathbf{w}$ and $\mathbf{w}^T$ to $\mathbf{Y}_{e1}\varepsilon_d$, the accuracy of calculated results of (25) can be evaluated by

$$Error=\frac{|\varepsilon_d-\varepsilon_0|}{|\lambda_d|}\left|\frac{\partial\lambda_d}{\partial\rho_d}\mathbf{w}\left(\mathbf{Y}_{e1}\right)\mathbf{w}^T\right|\times100\%,\ \varepsilon_0=0. \tag{28}$$

where $\mathbf{w}$ and $\mathbf{w}^T$ are left and right eigenvectors corresponding to ρ_d, respectively. $\partial\lambda_d/\partial\rho_d$ represents the sensitivity of λ_d to ρ_d.

Equation (28) shows that if the damping of λ_d is weaker, the accuracy of the proposed method is higher. In this study, initial value of ε_0 is zero because only the weak-damping DC voltage oscillation mode is focused in DC voltage oscillation stability analysis. Obviously, accuracy of the method can be improved if ε_d can be approximately predicted or multiple rounds of iterative calculation can be carried out so that ε_0 can be closed to ε_d.

F. Comparison with other modal calculation methods

Table I
Compared Results of Five Different Modal Calculation Methods

Methods	Highest Dimension	Accuracy	Cause of errors
①	*NH+T*	Highest	None.
②	*T*	Low	Ignoring dynamics of VSCs.
③	NH_r+T	High	Ignoring fast dynamics of VSCs.
④	*H*+1	Medium	Ignoring differences of VSCs.
⑤	*H*+1	High	Using $j\omega_d$ represents λ_d.

Note: The orders of the DC-voltage-droop-controlled VSC and the DC network are H and T, respectively. H_r is the dimension of the reduced-order model of a VSC using the method ③, and $H_r<H$.

The compared results are summarized in Table I. Five modal calculation methods are involved in this comparative analysis.

Method ①: Full-order model-based method. The calculated results are the most accurate since comprehensive dynamics of the MTDC distribution system are considered. However, as the number of VSCs increases, using full-order model may result in time-consuming.

Method ②: Reduced-order model-based method proposed in [3]. The dimension of the model is reduced since dynamics of VSCs are fully ignored. Thus, the method can only be applied to analyze the instability caused by the droop coefficients and DC lines. It is invalid in DC voltage stability analysis.

Method ③: Reduced-order model-based method proposed in [29]. The singular perturbation technique is used to reduce the dynamic order of a VSC, so that the dimension of the model is less than that of the full-order model. However, as the number of VSCs increases, the dimension of this reduced-order model still increases. The curse of dimensionality still occurs as long as the number of converters is large.

Method ④: Reduced-order model-based method proposed in [36]. The dynamics of multiple VSCs are equivalent to a VSC using similarity transformation technique, thus the dimension of this reduced-order model is significantly reduced. However, the VSCs involved in the calculation should be assumed to be same,

which is difficulty to be applied in actual.

Method ⑤: Reduced-order model-based method proposed in this study. The dynamic reconstruction technique is used so that the assumption of the method ④ is removed. The dimension of this reduced-order model is same as that of the method ④ while the accuracy is significantly improved, which is explained in detail as follows.

Regarding the method proposed in [36], a standard model of VSCs must first be determined to represent the dynamics of all VSCs, with the assumption that all VSCs are same. However, the dynamics of the VSCs actually differ according to their control parameters and operating states, which renders the selection of a standard VSC difficult. Since the accuracy of the calculated results not only depends on the reduced-order method, but also on the choice of the standard model, a bad choice may result in less accurate calculation results. For several VSCs, making the proper choice is time-consuming. In contrast, the method proposed in this study preserves the dynamics of the VSCs by using the dynamic reconstruction technique. Therefore, no matter which VSC is selected as the standard VSC, the dynamics cannot be ignored. Consequently, the choice of the standard VSC has only a slight effect on the calculation accuracy.

Moreover, the differences among VSCs are ignored using the method proposed in [36], which presents difficulties for accurately determining the oscillation mode in real-world systems. However, the method proposed in this study considers the differences of the VSCs, and the highest dimensional order of the calculation remains the same. Therefore, the method proposed in this paper can be widely applied to real-world engineering projects.

IV. THREE-TERMINAL DC DISTRIBUTION SYSTEM EXAMPLE

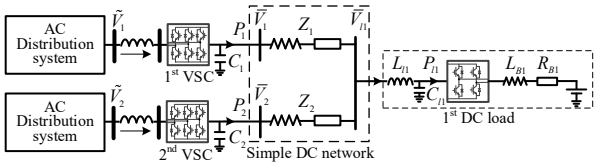

Fig. 6. Three–terminal DC distribution system.

In the first example, single DC bus configuration is adopted, DC loads are represented by an aggregated DC load, and two AC distribution systems are connected to the DC distribution system for power supply. Various operating states and control parameters are considered and further verified in experimental platform. Therefore, it is sufficient to demonstrate practicability of the proposed method. In Fig. 6, the 1st and 2nd VSCs use DC voltage droop control, and the DC-DC converter of the DC load adopts active power control so that the dynamics of the DC load are equal to that of the constant power load (CPL). The detailed system parameters are provided in Table B1 in Appendix B.

A. Dynamic-Reconstruction-Based Reduced-Order Modal Calculation of the DC Voltage Oscillation Mode

To present the calculation process of the proposed method, $G_{ik}(s)$ is temporarily assumed as 1. It should be noted that is not a necessary condition for calculating the DC voltage oscillation mode. Accordingly, the transfer functions of the VSCs in DC voltage timescale are obtained as follows:

$$\begin{aligned}\Delta\bar{V}_1 &= \frac{1.001s+0.0032}{6.594s^2+0.6949s+0.1611}=R_{e1}(s)\Delta\bar{I}_{net1}\\ \Delta\bar{V}_2 &= \frac{1.022s+0.0135}{6.732s^2+0.6127s+0.2709}=R_{e2}(s)\Delta\bar{I}_{net2}\end{aligned}. \quad (29)$$

The admittance matrix of the DC network is obtained as follows:

$$\begin{bmatrix}\bar{I}_{net1}\\ \bar{I}_{net2}\\ \bar{I}_{netl1}\end{bmatrix}=-\begin{bmatrix}Z_1^{-1} & 0 & -Z_1^{-1}\\ 0 & Z_2^{-1} & -Z_2^{-1}\\ -Z_1^{-1} & -Z_2^{-1} & Z_1^{-1}+Z_2^{-1}\end{bmatrix}\begin{bmatrix}\bar{V}_1\\ \bar{V}_2\\ \bar{V}_{l1}\end{bmatrix} \quad (30)$$

where $Z_1=0.06677s+0.03562$ and $Z_2=0.178s+0.095$.

The 1st VSC is selected as the standard VSC, such that

$$R_{e0}(s)=\frac{1.001s+0.0032}{6.594s^2+0.6127s+0.1611}. \quad (31)$$

The reconstructed impedances are obtained from (20), (29) and (31) as

$$\begin{aligned}&\Delta R_{e1,1}(s)^{-1}=0, \Delta R_{e2,1}(s)=0\\ &\Delta R_{e1,2}(s)=\frac{1.001s+0.0032}{0.138s^2-0.0822}\\ &\Delta R_{e2,2}(s)=\frac{0.021s+0.0103}{6.594s^2+0.6949s+0.1611}\end{aligned}. \quad (32)$$

From (30) and (32), at the DC voltage oscillation frequency of 53.6 rad/s (obtained by FFT analysis), the admittance matrix of the reconstructed DC network is obtained as follows:

$$\begin{bmatrix}\bar{I}_{net1}\\ \bar{I}_{net2}\end{bmatrix}=\begin{bmatrix}22.839+j2.688 & -23.981-j1.744\\ -23.981-j1.744 & 23.916+j0.997\end{bmatrix}\begin{bmatrix}\bar{V}_1\\ \bar{V}_2\end{bmatrix}. \quad (33)$$

The eigenvalue of the admittance matrix corresponding to DC voltage oscillation mode is $-0.5937+j0.1167$, and thus, the characteristic equation is obtained from (25) as follows:

$$7.4298s^2+0.1038s+0.1597=0. \quad (34)$$

From (34), the DC voltage oscillation mode is calculated to be $\lambda_F=\omega_0(-0.00699+j0.14644)=-2.63+j55.2$ (rad/s).

B. Accuracy of the calculated results

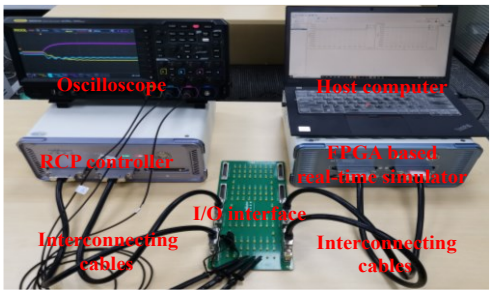

Fig. 7. Experimental platform of the DC distribution system

For confirmation, full-order state-space matrix of the MTDC

distribution system is established and the DC voltage oscillation mode is calculated as – 2.15 + *j*53.76. It can be seen from (35) that the error in the calculated result is 2.82 %, which is accurate for stability analysis.

$$error = \frac{|\lambda_F - \lambda_R|}{|\lambda_R|} = \frac{|-0.48 + j1.44|}{|-2.15 + j53.76|} = 2.82\% . \quad (35)$$

In addition, to further verify the accuracy of the calculated results, an experimental three–terminal DC distribution system is established in HIL lab, as shown in Fig.7. The FPGA-based power electronics real-time simulation experiment platform is a complete closed-loop system of a MT 6020 simulator and a MT 1050 controller. Detail parameters are given in Table II.

Table II
Parameters of the experimental DC distribution system

Parameters	Value
Number of bridge arms of the VSC	3
Power electronic device used in the VSC	IGBT
Nominal DC bus voltage	500 V
Nominal power	100 kW
DC capacitance	7000 μF
Parameters of the transmission line, Z_1	0.09 Ω, 0.44 mH
Parameters of the transmission line, Z_2	0.24 Ω, 1.18 mH
Simulation time step	1 μs
Control sample time	100 μs
Switching frequency	5 kHz

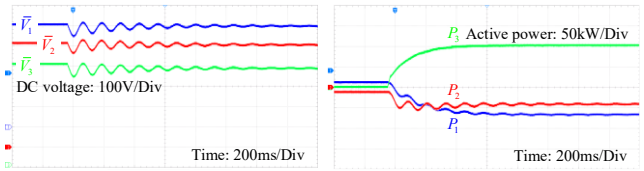

(a) (b)

Fig. 8. Experimental results. (a) DC voltage. (b) Output active power

At 0.36 s, the active power of the DC load increases from 0 kW to 100 kW. The experimental results are illustrated in Fig. 8. The data between 1 s and 2 s is used for Prony analysis using Prony Tool Box of the MATLAB [40]. The results indicate that the DC voltage oscillation mode is – 2.2 + *j*51.5, which is close to the calculated result of the reduced-order model.

C. Comparison Study

To demonstrate the advantages of the proposed method, the modal calculation methods introduced in section III *F* are compared numerically in this section. Here, an index is simply defined as the degree of the differences between the VSCs.

$$D_f = \sum_{k=1}^{N} \left(\frac{\sum_{i=1}^{2} \left(z_{i,k} - z_{i,\min} \right) + \sum_{j=1}^{3} \left(g_{j,k} - g_{j,\min} \right)}{\sum_{i=1}^{2} z_{i,\min} + \sum_{j=1}^{3} g_{j,\min}} \right) \quad (36)$$

where, $z_{i,\min}$ and $g_{j,\min}$ are minimum values of $z_{i,k}$ and $g_{j,k}$, respectively, $i = 1, 2$, $j = 1, 2, 3$, and $k = 1, 2, \ldots, N$.

Table III indicates that the calculated results using reduced-order methods ③, ④, and ⑤ are extremely close to the actual results when all DC-voltage-droop-controlled VSCs are identical (D_f = 0%). Regarding method ③, only fast VSC dynamics that slightly affect the calculated results are ignored, so the DC voltage oscillation mode can be accurately obtained. Under the condition that D_f = 0%, method ④ is same as method ⑤, and they do not ignore any dynamics, so that the calculated results are more accurate than other reduced-order methods. However, using method ② cannot obtain the DC voltage oscillation mode because most dynamics of the VSCs are ignored. These results indicate that using a reduced-order method without considering VSC dynamics is invalid in calculating the DC voltage oscillation mode.

As the differences of the VSCs increase, the accuracy of the calculated results decreases. Method ③ is slightly affected by variation of the differences. It is the most accurate but has the highest calculational dimension among methods ② – ⑤. Method ④ has worse accuracy than method ⑤ because the latter considers the effects of the VSC differences using the dynamic reconstruction technique. Under the condition that D_f = 6%, the maximum calculation error of method ④ is 26.03%, while that of method ⑤ is 2.82%. These results confirm that the dynamic

Table III
Calculated Results of Different Adopted Methods

D_f = 0%			
Methods	Standard VSC	DC voltage oscillation mode	Error
①	–	–1.96 + *j*66.94	0.00%
②	–	–	100%
③	–	–2.16 + *j*66.96	0.30%
④	1st VSC	–1.92 + *j*66.98	0.08%
	2st VSC	–1.92 + *j*66.98	0.08%
⑤	1st VSC	–1.92 + *j*66.98	0.08%
	2st VSC	–1.92 + *j*66.98	0.08%
D_f = 2%			
Methods	Standard VSC	DC voltage oscillation mode	Error
①	–	–2.69 + *j*62.51	0.00%
②	–	–	100%
③	–	–2.86 + *j*62.52	0.30%
④	1st VSC	–3.58 + *j*57.75	7.74%
	2st VSC	–1.95 + *j*66.97	7.23%
⑤	1st VSC	–2.30 + *j*63.09	1.12%
	2st VSC	–3.19 + *j*62.59	0.81%
D_f = 6%			
Methods	Standard VSC	DC voltage oscillation mode	Error
①	–	–1.87 + *j*54.81	0.00%
②	–	–	100%
③	–	–2.13 + *j*55.01	0.60%
④	1st VSC	–4.16 + *j*40.72	26.03%
	2st VSC	1.47 + *j*66.50	22.17%
⑤	1st VSC	–1.95 + *j*56.07	2.30%
	2st VSC	–0.79 + *j*55.92	2.82%

reconstruction technique improves the accuracy and can be used to accurately calculate DC voltage oscillation mode in realistic scenarios, even when different VSCs are involved. In addition, when method ④ is adopted, choosing the 1st VSC as the standard can improve the accuracy of the calculated results by 4%, which indicates that the choice of the standard VSC may affect calculation errors. However, when method ⑤ is adopted, no significant variation in the error is observed, irrespective of which VSC is chosen as the standard, indicating that calculation accuracy is only slightly related to the choice of a standard VSC.

When the power of the DC load increases from 0.1 to 1.75 p.u., the trajectories of the DC voltage oscillation mode are calculated using different methods as shown in Fig. 9. It can be seen that increasing the power of the DC load reduces the DC voltage oscillation stability, as the DC voltage oscillation mode

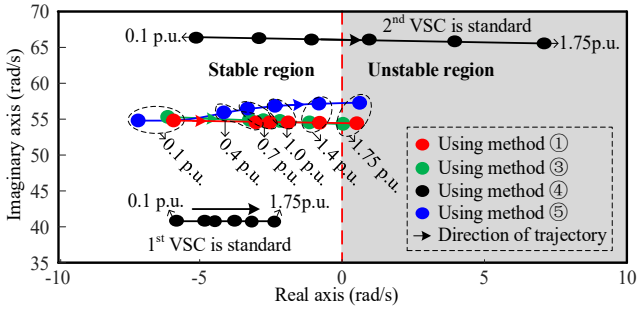

Fig. 9. Trajectories when the DC load power increases from 0.1 to 1.75 p.u.

moves to the right side of the complex plane. The DC voltage oscillation mode is calculated as 0.36 + *j*53.64 when the power of the DC load increases to 1.75 p.u using method ①, indicating that the realistic DC voltage oscillation is unstable. In addition, the occurrence of the instability can also be correctly determined using the reduced-order methods ③ and ⑤.

However, if the DC voltage oscillation mode is calculated using method ④, the analyzed results contain errors. If the 1st VSC is selected as the standard, the DC voltage oscillation mode is calculated to be –2.23 + *j*40.58 when the power of the DC load is 1.75 p.u., which leads to the erroneous conclusion that the DC voltage oscillation is stable. If the 2nd VSC is selected as the standard, the DC voltage oscillation mode is calculated to be 0.87 + *j*66.75 when the power of the DC load increases to 1 p.u., and the DC voltage oscillation is considered to be unstable. This is an incorrect result, as the realistic DC voltage is stable with the oscillation mode that is –1.87 + *j*54.81. It verifies that ignoring the differences of VSCs can result in misjudgments about the DC voltage oscillation stability.

When the power of the DC load increases from 0.1 to 1.75 p.u., the trajectory of the DC voltage oscillation mode using method ⑤ (1st VSC is selected as standard) is indicated by the blue line in Fig. 9. The DC voltage oscillation mode is calculated to be 0.44 + *j*55.67 (1st VSC is selected as standard) and 0.05 + *j*54.92 (2nd VSC is selected as standard) when the power of the DC load is 1.75 p.u. This demonstrates that the accuracy of the calculated results is significantly improved compared with method ④. Moreover, the choice of the standard VSC does not significantly affect the calculated results, so that the DC voltage oscillation stability can be correctly determined. The calculated results using method ③ are also accurate, but its calculational dimensions are higher than that of method ⑤. Therefore, the method proposed in this study is more accurate than the old method ④, and retains the advantage of low-order calculational dimensions for determining the DC voltage oscillation stability when the VSCs are different.

V.A LARGE-SCALE EXAMPLE

This simulation addresses a large-scale MTDC distribution system that adopts DC voltage droop control. A hybrid network composed of multi-bus and ring bus configurations is used for examinations. The MTDC distribution system has four regions, and each region contains twenty-five grid-connected VSCs. They delivery power from distributed wind turbines or/and AC distribution systems to two DC loads. Its configuration is shown in Fig. 10.

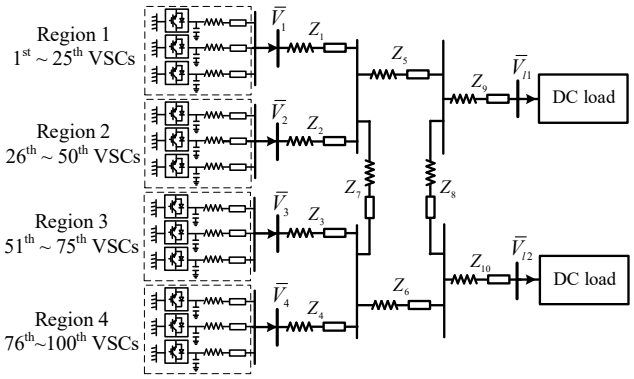

Fig. 10. MTDC distribution system connected with 100 VSCs.

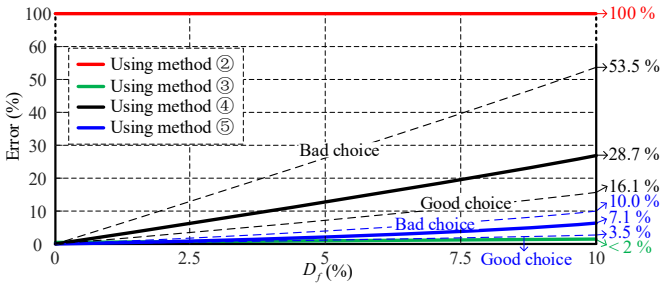

Fig. 11. Trajectories of the calculated errors when D_f increases.

In Fig. 10, the control parameters and steady states of VSCs are different. Here, D_f is used to describe the degree of the difference among the VSCs. When methods ④ and ⑤ are used, the calculation error changes with different choices of the standard VSC, even if D_f is the same. Therefore, a hundred tests were made in a specific scenario, so that each VSC can be selected as the standard once. The test that has a maximum calculation error is defined as 'bad choice' and that has a minimum calculation error is defined as 'good choice', which are indicated by dotted lines in Fig. 11. The average errors in the calculated results are illustrated by solid lines in Fig. 11.

Fig. 11 show that the calculation error rarely varies using methods ② and ③. Method ② is invalid since too many dynamics of the VSCs are ignored for reducing the calculational

order. The DC voltage oscillation mode cannot be obtained so the error is 100% in any case. The error of method ③ is less than 2% because the ignored fast dynamics only slightly affect the calculated results. However, the calculational dimension is not reduced significantly using method ③. The errors of methods ④ and ⑤ increase with increasing D_f, but the results of method ⑤ are always more accurate than method ④. At D_f = 10%, method ④ is nearly invalid because it results in a 30% deviation from the actual results; in the worst case, the error exceeds 50%. However, method ⑤ only provides a deviation of 7%; in the worst case, the error does not exceed 10%. These results demonstrate that the choice of the standard VSC has more significant effects on the calculated results when method ④ is adopted, but the effects can be reduced by using method ⑤. The engineering control parameters are similar between different VSCs since they are normally designed by a particular company. Therefore, the differences are mainly caused by power flow. We obtained a value of D_f < 5% in most of our tests, which suggests that the proposed method is accurate and effective for analyzing the DC voltage oscillation stability of most real-world engineering projects.

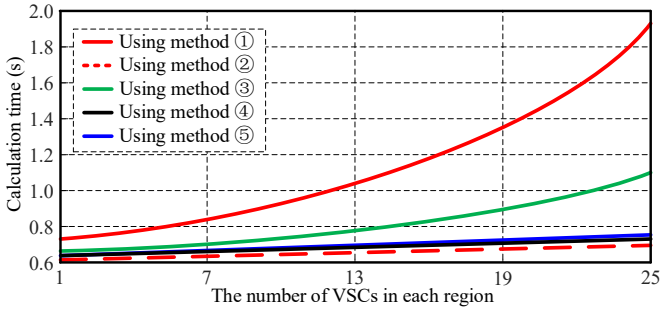

Fig. 12. Calculation time using different models, with increasing number of VSCs in each region.

The modal calculation times of different methods were examined using MATLAB (2020a) and Intel (R) Core (TM) i9-9980HK CPU @ 2.40GHz. Increasing the number of VSCs from 1 to 25 in each region, the computation time is illustrated in Fig. 12. The calculation time increases with the increasing number of VSCs. The most time-consuming model is the full-order model because the dimensions of the full-order model are always higher than that of the reduced-order model. The computation time is reduced when reduced-order methods are adopted. However, the calculation time of method ③ still increases significantly as the number of VSCs increases. Unlike methods ① and ③, the calculation time of methods ②, ④, and ⑤ is faster and increases only slightly as the number of VSCs increases. The reason is that the maximum calculational dimension of methods ②, ④, and ⑤ is mainly associated with the dimension of the DC network, which increases by 1 when a VSC is connected. However, when methods ① and ③ are used, increasing the number of VSCs directly increases the maximum calculation dimensions of the DC distribution system's state-space model, leading to an exponential increase in computation time. Therefore, the growth rate of the maximum dimension using reduced-order methods ②, ④, and ⑤ is much slower than that using methods ① and ③. Method ⑤ provides at least a 60% reduction in computation time compared with method ① when the number of VSCs in each region is 25.

Although the maximum dimension of methods ④ and ⑤ is the same, the computation time of method ④ is slightly lower than that of method ⑤. This is because some extra low-order equations are involved in constructing the dynamics of the VSCs and DC network, which requires a small amount of computation time. Therefore, Fig. 11 and Fig. 12 show that the reduced-order method proposed in this study is an accurate and rapidly approach to investigating DC voltage oscillation stability of the complex MTDC distribution system.

VI. Conclusion

When considering the expansion of a DC distribution system, many sources are connected to it with AC/DC converters to avoid energy conversion of the DC load. A DC voltage droop control is normally adopted to control DC voltage and share power among multiple VSCs. To determine the small-signal stability of the DC voltage of the large-scale DC distribution system, the DC oscillation mode should first be calculated. However, the dimensionality of such a complex system is prohibitively high for modal computations, thus necessitating reduced-order modal computations to investigate DC voltage oscillation stability.

In this paper, a dynamic reconstruction technique is proposed to fully consider the differences of the VSCs induced by control parameters or/and steady states. Based on that, a reduced-order modal computation method is proposed to accurately calculate the weak-damping DC voltage oscillation modes, and thus determine the DC voltage oscillation stability. In a departure from traditional reduced-order modal calculation methods, the proposed method does not assume that VSCs are either identical or with a specified topology. As the number of VSCs increases, the highest dimension increases slowly. Therefore, this method is effective for real-world engineering applications and provides more accurate results.

The contributions of this study are summarized as follows.

1) The proposed dynamic reconstruction technique proves that the differences of VSCs can be considered as impedances added to the DC network. Therefore, the dynamics of different VSCs can be comprehensively considered, improving the accuracy of the calculated results.

2) The proposed reduced-order modal calculation method is highly accurate in DC voltage stability analysis, has a low-dimensionality order and is computationally efficient. The weak-damping DC voltage oscillation mode can be accurately calculated, and rapidly determines the stability. The highest calculational dimension is low and increases slowly as the number of VSCs increases.

3) The proposed reduced-order modal calculation method is more advanced than the other reduced-order methods in DC voltage stability analysis. Comparisons with the other reduced-order methods proposed in [3] and [36], show that the calculated results are more accurate while the calculation times are similar. Comparisons with the reduced-order methods

proposed in [29], the calculation error is within 5% for a large real-world engineering project with D_f < 5%, while the calculation time is significantly reduced. Therefore, it is more suitable for DC voltage oscillation stability analysis of actual large real-world DC distribution systems such as the DC system connected with multiple VSCs as shown in Fig.8.

In further work, the causes of the error of the proposed method will be investigated in depth, and some techniques mentioned in section III F will be examined to improve the accuracy. Then, more specific scenarios that are suitable for this method, such as DC distribution systems with different dc-dc converters will be explored.

APPENDIX A

At the DC voltage oscillation frequency ω_d, substituting $s = j\omega_d$ in to $\mathbf{Y}_e(s)$, dynamics of the DC network can be represented by $\mathbf{Y}_e(\omega_d)$, yields

$$\mathbf{Y}_d(\omega_d)\mathbf{F}_e(s) + \mathbf{E} = \mathbf{0}. \tag{37}$$

Denote a matrix $\mathbf{P}$, such that

$$\mathbf{P}\mathbf{Y}_d(\omega_d)\mathbf{P}^{-1} = \begin{bmatrix} \rho_{R1} + j\rho_{M1} & & \\ & \rho_{Rk} + j\rho_{Mk} & \\ & & \rho_{RN} + j\rho_{MN} \end{bmatrix} \tag{38}$$

Multiply $\mathbf{P}$ and $\mathbf{P}^{-1}$ to (37), yields

$$\begin{aligned} &\mathbf{P}\mathbf{Y}_d(\omega_d)\mathbf{F}_e(s)\mathbf{P}^{-1} + \mathbf{P}\mathbf{E}\mathbf{P}^{-1} = \mathbf{0} \\ &= \mathbf{P}\mathbf{Y}_d(\omega_d)\mathbf{P}^{-1}\mathbf{F}_e(s) + \mathbf{E} \\ &= \begin{bmatrix} R_{e0}(s)(\rho_{R1} + j\rho_{M1}) + 1 & & \\ & \ddots & \\ & & R_{e0}(s)(\rho_{RN} + j\rho_{MN}) + 1 \end{bmatrix} \end{aligned} \tag{39}$$

Convert $j\rho_{Mk}$ to s, it has

$$\begin{cases} R_{e0}(s)(\rho_{R1} + \dfrac{\rho_{M1}}{\omega_d}s) + 1 = 0 \\ \vdots \\ R_{e0}(s)(\rho_{RN} + \dfrac{\rho_{MN}}{\omega_d}s) + 1 = 0 \end{cases}. \tag{40}$$

Thus, (17) can be represented by multiple sub–equations in (40). Considering the eigenvalue corresponding to the DC voltage oscillation mode is ρ_0. The DC voltage oscillation can be calculated by

$$R_{e0}(s)\left[\rho_{R0} + \rho_{M0}s\right] + 1 = 0 \tag{41}$$

where $\rho_{R0} = \mathrm{Re}[\rho_0]$, $\rho_{M0} = \mathrm{Im}[\rho_0]/\omega_d$.

APPENDIX B

Table IV
Parameters of the Three–Terminal DC Distribution System

Parameters and operating states of the VSCs	Values
Active power output from the 1st VSC	0.62 *p.u.*
Active power output from the 2nd VSC	0.42 *p.u.*
DC voltage of the 1st VSC	0.9995 *p.u.*
DC voltage of the 2nd VSC	1.0165 *p.u.*
Active power of the DC load	1.00 *p.u.*
Capacitors at the DC side of the VSCs	6.59 *p.u.*
Control parameters of the 1st VSC	$K_{a1} = 0.01, K_{d1} = 0.5$, $K_{p1} = 0.1, K_{i1} = 120/\omega_0$, $K_{p1}^c = 0.1, K_{i1}^c = 500/\omega_0$.
Control parameters of the 2nd VSC	$K_{a2} = 0.05, K_{d2} = 1$, $K_{p2} = 0.1, K_{i2} = 100/\omega_0$, $K_{p2}^c = 0.1, K_{i2}^c = 500/\omega_0$.

REFERENCES

[1] R. Ahmadi and M. Ferdowsi, "Improving the performance of a line regulating converter in a converter-dominated DC microgrid system," *IEEE Trans. Smart Grid*, vol. 5, no. 5, pp. 2553–2563, Sep. 2014.

[2] L. Zhang, B. Tong, and Z. Wang, et al., "Optimal Configuration of Hybrid AC/DC Distribution Network Considering the Temporal Power Flow Complementarity on Lines," *IEEE Trans. Smart Grid*, to be published.

[3] S. Anand and B. G. Fernandes, "Reduced-Order Model and Stability Analysis of Low-Voltage DC Microgrid," *IEEE Trans. Ind. Electron.*, vol. 60, no. 11, pp. 5040-5049, Nov. 2013.

[4] E. Pritchard, D. C. Gregory and S. Srdic, "The dc Revolution," *IEEE Electrific. Mag.*, vol. 4, no. 2, pp. 4-9, Jun. 2016.

[5] T. Dragicevic, J. C. Vasquez and J. M. Guerrero, et al., "Advanced LVDC Electrical Power Architectures and Microgrids," *IEEE Electrific. Mag.*, vol. 2, no. 1, pp. 54-65, Mar. 2014.

[6] Q. Fu, W. Du, and H. F. Wang, "Planning of the DC System considering Restrictions on Small Signal Stability of EV Charging Stations and Comparison between Series and Parallel Connections," *IEEE Trans. Veh. Technol.*, vol. 69, no. 10, pp. 10724-10735, Oct. 2020.

[7] F. Nejabatkhah and Y. W. Li, "Overview of power management strategies of hybrid AC/DC microgrid," *IEEE Trans. Power Electron.*, vol. 30, no. 12, pp. 7072–7089, Dec. 2015.

[8] Z. Li and M. Shahidehpour, "Small-Signal Modeling and Stability Analysis of Hybrid AC/DC Microgrids," *IEEE Trans. Smart Grid*, vol. 10, no. 2, pp. 2080-2095, Mar. 2019.

[9] K. Yukita, "AC/DC microgrids," In Integration of Distributed Energy Resources in Power Systems. London: Academic Press, 2016, pp. 236-260.

[10] E. Rodriguez-Diaz, F. Chen and J. C. Vasquez, et al., "Voltage-Level Selection of Future Two-Level LVdc Distribution Grids: A Compromise Between Grid Compatibiliy, Safety, and Efficiency," *IEEE Electrific. Mag.*, vol. 4, no. 2, pp. 20-28, Jun. 2016.

[11] M. Qu, T. Ding, L. Huang and X. Wu, "Toward a Global Green Smart Microgrid: An Industrial Park in China," *IEEE Electrific. Mag.*, vol. 8, no. 4, pp. 55-69, Dec. 2020.

[12] K. Rouzbehi, A. Miranian, and J. I. Candela, et al., "A Generalized Voltage Droop Strategy for Control of Multiterminal DC Grids," *IEEE Trans. Ind. Appl.*, vol. 51, no. 1, pp. 607-618, Jan. 2015.

[13] T. Morstyn, B. Hredzak and V. G. Agelidis, "Control Strategies for Microgrids With Distributed Energy Storage Systems: An Overview," *IEEE Trans. Smart Grid*, vol. 9, no. 4, pp. 3652-3666, July 2018.

[14] T. Dragicevic, P. Wheeler, and F. Blaabjerg, "DC distribution systems and microgrids,". London: The Institution of Engineering and Technology, 2018, pp. 13-40.

[15] J. M. Guerrero, M. Chandorka, T. Lee, and P. C. Loh, "Advanced control architectures for intelligent microgrids—Part I: Decentralized and hierarchical control," *IEEE Trans. Ind. Electron.*, vol. 60, no. 4, pp. 1254–1262,Apr. 2012.

[16] L. Meng, Q. Shafiee and G. F. Trecate, et al., "Review on Control of DC Microgrids and Multiple Microgrid Clusters," *IEEE Trans. Emerg. Sel. Topics Power Electron.*, vol. 5, no. 3, pp. 928-948, Sept. 2017.

[17] D. Niyato, L. Xiao, and P. Wang, "Machine-to-machine communications for home energy management system in smart grid," *IEEE Commun. Mag.*, vol. 49, no. 4, pp. 53–59, Apr. 2011.

[18] A. Gupta, S. Doolla and K. Chatterjee, "Hybrid AC–DC Microgrid: Systematic Evaluation of Control Strategies," *IEEE Trans. Smart Grid*, vol. 9, no. 4, pp. 3830-3843, July 2018.

[19] C. Gavriluta, J. I. Candela, and C. Citro, et al., "Decentralized Primary Control of MTDC Networks With Energy Storage and Distributed Generation," *IEEE Trans. Ind. Appl.*, vol. 50, no. 6, pp. 4122-4131, Nov. 2014.
[20] M. Davari and Y. A. I. Mohamed, "Robust Droop and DC-Bus Voltage Control for Effective Stabilization and Power Sharing in VSC Multiterminal DC Grids," *IEEE Trans. Power Electron.*, vol. 33, no. 5, pp. 4373-4395, May 2018.
[21] M. Farrokhabadi, C. A. Cañizares and J. W. Simpson-Porco, et al., "Microgrid Stability Definitions, Analysis, and Examples," *IEEE Trans. Power Syst.*, vol. 35, no. 1, pp. 13-29, Jan. 2020.
[22] M. Farrokhabadi, S. Konig, C. Cañizares, K. Bhattacharya, and T. Leibfried, "Battery energy storage system models for microgrid stability analysis and dynamic simulation," *IEEE Trans. Power Syst.*, vol. 33, no. 2, pp. 2301–2312, Aug. 2017.
[23] L. Guo, P. Li and X. Li, et al., "Reduced-order modeling and dynamic stability analysis of MTDC systems in DC voltage control timescale," *CSEE Journal of Power and Energy Systems,* vol. 6, no. 3, pp. 591-600, Sept. 2020.
[24] Y. Ito, Y. Zhongqing, and H. Akagi, "DC microgrid based distribution power generation system," *Proc. 4th Int. Power Electron. Motion Control Conf.* (IPEMC), Aug. 2004, pp. 1740–1745.
[25] L. Herrera, E. Inoa and F. Guo, et al., "Small-Signal Modeling and Networked Control of a PHEV Charging Facility," *IEEE Trans. Ind. Appl.*, vol. 50, no. 2, pp. 1121-1130, Mar. 2014.
[26] M. Tabari and A. Yazdani, "Stability of a dc Distribution System for Power System Integration of Plug-In Hybrid Electric Vehicles," *IEEE Trans. Smart Grid*, vol. 5, no. 5, pp. 2564-2573, Sept. 2014.
[27] H. Yuan, X. Yuan and J. Hu, "Modeling of Grid-Connected VSCs for Power System Small-Signal Stability Analysis in DC-Link Voltage Control Timescale," *IEEE Trans. Power Syst.*, vol. 32, no. 5, pp. 3981-3991, Sept. 2017.
[28] M. Rasheduzzaman, J. A. Mueller and J. W. Kimball, "Reduced-Order Small-Signal Model of Microgrid Systems," *IEEE Trans. Sustain. Energy*, vol. 6, no. 4, pp. 1292-1305, Oct. 2015.
[29] I. P. Nikolakakos, H. H. Zeineldin, and M. S. El-Moursi, et al., "Stability Evaluation of Interconnected Multi-Inverter Microgrids Through Critical Clusters," *IEEE Trans. Power Syst.*, vol. 31, no. 4, pp. 3060-3072, July 2016.
[30] Y. Wang, C Lu, and L Zhu, et al., "Comprehensive modeling and parameter identification of wind farms based on wide-area measurement systems," *J. Mod. Power Syst. Clean Energy*, vol. 4, no. 3, pp. 383–393, 2016.
[31] M. Ali, I. Ilie, J. V. Milanović and G. Chicco, "Probabilistic clustering of wind generator," *in Proc. IEEE PES General Meeting, Providence*, RI, USA, Jul. 2010, pp. 1–6.
[32] J. Zou, C. Peng, H. Xu, and Y. Yan, "A fuzzy clustering algorithm-based dynamic equivalent modeling method for wind farm with DFIG," *IEEE Trans. Energy Convers.*, vol. 30, no. 4, pp. 1329–1337, May 2015.
[33] Y Zhou, L Zhao, and W Lee, "Robustness analysis of dynamic equivalent model of DFIG wind farm for stability study," *IEEE Trans. Ind. Appl.*, vol. 54, no. 6, pp. 5682–5690, Nov. 2018.
[34] I. Erlich, F. Shewarega, and C. Feltes, et al., "Determination of dynamic wind farm equivalents using heuristic optimization," *in Proc. IEEE PES General Meeting*, San Diego, CA, USA, Jul. 2012, pp. 1–8.
[35] P. Wang, Z. Zhang, and Q. Huang, et al., "Improved wind farm aggregated modeling method for large-scale power system stability studies," *IEEE Trans. Power Syst.*, vol. 33, no. 6, pp. 6332–6342, Nov. 2018.
[36] W. Du, W. Dong and H. Wang, "A Method of Reduced-Order Modal Computation for Planning Grid Connection of a Large-Scale Wind Farm," *IEEE Trans. Sustain. Energy*, vol. 11, no. 3, pp. 1185-1198, July, 2020.
[37] K. E. Lucas et al., "Robust Control of Interconnected Power Electronic Converters to Enhance Performance in DC Distribution Systems: A Case of Study," *IEEE Trans. Power Electron.*, vol. 36, no. 4, pp. 4851-4863, April 2021.
[38] L. E. Zubieta, "Are Microgrids the Future of Energy?: DC Microgrids from Concept to Demonstration to Deployment," *IEEE Electrific. Mag.*, vol. 4, no. 2, pp. 37-44, June 2016.
[39] P. Vorobev, P. Huang, and M. Al Hosani, et al., "High-Fidelity Model Order Reduction for Microgrids Stability Assessment," *IEEE Trans. Power Syst.*, vol. 33, no. 1, pp. 874-887, Jan. 2018.
[40] Satnam Singh. (2021). Prony Toolbox. MATLAB Central File Exchange. [Online]. Available: https://www.mathworks.com/matlabcentral/fileexchange/3955-prony-toolbox. Retrieved November 18, 2021.